(e, 2e)-Spectroscopy and the Electronic Structure of Molecules. A Short Review with Selected Examples *

M. A. Coplan

Institute for Physical Science and Technology, University of Maryland, College Park, Maryland, USA

J. H. Moore and J. A. Tossell

Department of Chemistry and Biochemistry, University of Maryland, College Park, Maryland, USA

Z. Naturforsch. **48a**, 358–370 (1993); received January 30, 1992

The simple plane wave target Hartree-Fock impulse approximation for the (e, 2e) reaction is developed. One result of the approximation is the separation of the expression for the (e, 2e) cross-section into a kinematic factor and a structure factor that contains all of the information about the target. When the target is a molecule, the structure factor can be further separated into atomic terms and a geometric term. This is illustrated for a simple one-electron homonuclear diatomic molecule. Three examples of the application of (e, 2e) spectroscopy to systems of chemical interest are given. They are borazine (inorganic benzene), the methyl siloxanes and the inorganic complex trimethylamine–boron trifluoride.

Key words: (e, 2e)-Spectroscopy; Electron momentum spectroscopy; Electron momentum density; Electronic structure.

Introduction

(e, 2e)-spectroscopy has its origins in nuclear physics with the first experiments and theoretical analyses performed by physicists with a nuclear-physics background [1–3]. Once the feasibility of the experiments was demonstrated [4], chemists also became interested, and a large and increasing number of gas-phase molecules has been the subject of (e, 2e) studies [5]. In addition, (e, 2e)-spectroscopy has been applied to solid films [6, 7], crystals [8], and atoms in excited states [9]. The basic collision mechanism upon which (e, 2e)-spectroscopy is based has not been neglected, and there exists a large number of studies of the mechanism of the (e, 2e) reaction in different experimental geometries [10–12]. In this paper we will concentrate on the information that can be obtained from (e, 2e)-spectroscopy on the electronic structure of chemically interesting molecules. We will use three examples; borazine, sometimes called inorganic benzene, three siloxanes, and the weakly-bonded compound trimethylamine–boron trifluoride. The evolution of (e, 2e)-spectroscopy from an interesting curiosity to a worthwhile experimental technique for the investigation of the electronic structure of atoms and molecules is due in large part to the close relation between the experimental results and quantum-chemical calculations. Experimental data by themselves are not sufficient for a complete understanding of electronic structure because of the various averagings that are inherent in gas-phase experiments. On the other hand, calculations need experimental data to establish their validity. As we shall show, a close coupling between experiments and calculations can indeed tell a good deal about electronic structure and its relation to the chemical and physical properties of atoms and molecules.

We will begin with a brief review of the simple theory of the (e, 2e) reaction under conditions that are most relevant to electronic structure determinations. A more complete treatment of the theory has been given by Weigold and McCarthy [2]. We will then examine the experimental arrangements and the data analysis methods. Data on the three systems we have chosen as examples will be presented along with the calculations and interpretations.

Simple Theory of the (e, 2e) Reaction

The idea of the (e, 2e) reaction is simple and can be illustrated by a classical model, Figure 1. Assume that we have a single electron fixed in space, the target electron, and that we hit it with a second projectile

* Presented at the Sagamore X Conference on Charge, Spin and Momentum Densities, Konstanz, Fed. Rep. of Germany, September 1–7, 1991.

Reprint requests to Prof. Dr. M. A. Coplan, IPST-CSS Bldg., University of Maryland, College Park, MD 20742, USA.

0932-0784 / 93 / 0100-0358 $ 01.30/0. – Please order a reprint rather than making your own copy.

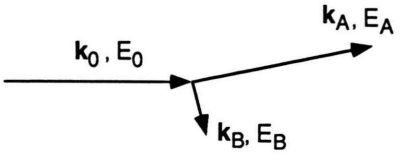

Fig. 1. Schematic diagram of a simple classical collision between two identical particles. The momenta and kinetic energies of the particles are indicated.

electron with kinetic energy E_0 and momentum $\boldsymbol{k}_0$. Energy and momentum are conserved so that the relations between the final energies, E_A and E_B, and final momenta $\boldsymbol{k}_A$ and $\boldsymbol{k}_B$ of the two electrons after the collision can be calculated. The momentum transferred to the target electron is $\boldsymbol{k}_0 - \boldsymbol{k}_A = \boldsymbol{K}$. For the simple situation described above, $\boldsymbol{K} = \boldsymbol{k}_B$ holds. In order to extend this simple picture, consider the target electron to be one of a number of electrons in an atom or molecule, with a binding energy I, and suppose that at the instant of collision with the projectile electron it is moving in some arbitrary direction with momentum $-\boldsymbol{q}$. Under these circumstances, the momentum of the target electron after the collision is the vector sum of the momentum transferred to it by the projectile electron and the momentum it had at the instant of the collision: $\boldsymbol{k}_B = \boldsymbol{k}_0 - \boldsymbol{k}_A - \boldsymbol{q}$ or $\boldsymbol{q} = \boldsymbol{k}_0 - \boldsymbol{k}_A - \boldsymbol{k}_B$. Furthermore, the sum of the kinetic energies of the projectile and target electrons after the collision are reduced by the value of the binding energy. The implications of this are profound. If one can measure the momenta of the incident electron before and after the collision, and that of the target electron after its ejection, it is possible to calculate the momentum of the target electron at the instant of collision directly. Additionally, the determination of the kinetic energies of the electrons after the collision is sufficient to establish the binding energy or ionization potential of the target electron. An orbital electron in an atom or molecule has a fixed ionization potential, and its momentum at any instant can be described by a momentum density function. By performing the collision experiment over and over with a collection of identical atoms or molecules and accepting for analysis only those electrons with a single ionization potential we can obtain this density function.

The momentum density of an electron in an atom or molecule is a fundamental quantum-mechanical property of the system and can be calculated from first principles. Our ability to measure momentum densities in a straightforward manner combined with binding-energy selectivity, is the most important feature of the (e, 2e) experiment.

The experimental configuration used in (e, 2e) experiments all share the same basic elements, a source of projectile electrons, energy/momentum analyzers, detectors for the scattered and target electrons and electronic circuits to distinguish the two electrons resulting from a single (e, 2e) event from all other electron-producing processes. In general, (e, 2e) experiments only measure a single component of $\boldsymbol{q}$, either the component that lies in the plane of the incident and scattered electron momentum vectors (coplanar geometry) or the component perpendicular to that plane (noncoplanar geometry). A third geometry, the symmetric out-of-plane one, combines elements of both the coplanar and noncoplanar geometries. The different geometries are listed in Table 1 along with the expressions for $|\boldsymbol{q}|$ as a function of the experimental parameters. The normal experimental parameter ranges are also listed.

In the gas phase all orientations of $\boldsymbol{q}$ are equally probable so that the determination of the momentum density of a single component of $\boldsymbol{q}$ is equivalent to a spherically-averaged momentum density. For oriented atoms or molecules it is possible to obtain momentum densities along preferred directions in space in a manner analogous to directional Compton profiles.

In the above discussion we have represented the collision process in classical terms while discussing the properties of the target electrons in the more quantum-mechanical language of distributions and densities. The quantum-mechanical treatment of the collision between the projectile and target electrons is most simply treated within the Born approximation with the incident, scattered, and ejected electrons are represented by plane waves. The interaction that connects the initial state and final state is taken to be the Coulomb interaction between the incident and target electrons. If the target electron is part of an atom or molecule, we can write the initial state of the system as the product of the wave function of the projectile electron and the many-electron wave function of the atom or molecule $\Psi(\boldsymbol{r}_1, \boldsymbol{r}_2, \ldots, \boldsymbol{r}_Z)$. The final state is the product of the wave functions of the scattered electron, ejected electron, and residual ion $\Phi(\boldsymbol{r}_1, \boldsymbol{r}_2, \ldots, \boldsymbol{r}_{Z-1})$.

$$\begin{aligned}
&\text{Initial state:} && e^{i\boldsymbol{k}_0 \cdot \boldsymbol{r}}\, \Psi(\boldsymbol{r}_1, \boldsymbol{r}_2, \ldots, \boldsymbol{r}_Z)\,, \\
&\text{Final state:} && e^{i\boldsymbol{k}_A \cdot \boldsymbol{r}}\, e^{i\boldsymbol{k}_B \cdot \boldsymbol{r}_B}\, \Phi(\boldsymbol{r}_1, \boldsymbol{r}_2, \ldots, \boldsymbol{r}_{Z-1})\,, \\
&\text{Interaction:} && \sum_{j=1}^{Z} \frac{-\varepsilon^2}{|\boldsymbol{r} - \boldsymbol{r}_j|} \quad \text{(two-body Coulomb operator)}\,. \qquad (1)
\end{aligned}$$

Table 1. Geometries in (e, 2e) experiments.

Geometry	Experimental constraints	Independent variable	Target momentum $\lvert\boldsymbol{q}\rvert$ (a.u.)[a]	Parameter range [b]
Symmetric noncoplanar	$E_A = E_B = E = (E_0 - I)/2$ $\theta_A = \theta_B = \theta$	ϕ	$2\sqrt{2}\left[\left(\sqrt{E}\cos\theta - \frac{\sqrt{E_0}}{2}\right)^2 + E\sin^2\theta\sin^2\frac{\phi}{2}\right]^{1/2}$	$E_0 = 400-2000$ eV $\theta = 45°$ $\phi = 0-60°$
Symmetric coplanar	$E_A = E_B = E = (E_0 - I)/2$ $\phi = 0$	$\theta = \theta_A = \theta_B$	$2\sqrt{2}\left[\left(\sqrt{E}\cos\theta - \frac{\sqrt{E_0}}{2}\right)^2\right]^{1/2}$	$E_0 = 400-2600$ eV $\theta = 30-60°$
Symmetric out-of-plane	$E_A = E_B = (E_0 - I)/2 = E$ $\theta' = \theta'_A = \theta'_B$ $\cos\theta\cos\phi = \cos\theta' = D$	$\phi' = \sin^{-1}(\tan\theta\sin\phi/2)$	$2\sqrt{2}\left[\left(\sqrt{E}\frac{D}{\cos\phi'} - \frac{\sqrt{E_0}}{2}\right)^2 + ED^2\tan^2\phi'\right]^{1/2}$	$E_0 = 800-2600$ eV $\theta = 44-45°$ $\phi' = 0-8°$
Asymmetric coplanar	$E_A \gg E_B$ $\theta_A \ll 1$ $\phi = 0$	θ_B	$2\left[\left(E_0 - \frac{I}{2}\right) + \sqrt{E_A E_B}(\cos\theta_A\cos\theta_B - \sin\theta_A\sin\theta_B\cos\phi) - \sqrt{E_0}(\sqrt{E_A}\cos\theta_A + \sqrt{E_B}\cos\theta_B)\right]^{1/2}$	$E_0 = 8000$ eV $E_B = 400-600$ eV $\theta_A = 10-17°$ $\theta_B = 30-140°$
Nonsymmetric coplanar (energy-sharing)	$E_0 = E_A + E_B + I$ $\theta_A = \theta_B = \theta$ $\phi = 0$	$\Delta E = E_A - E_B$	$\sqrt{2}\left[2E_0 - I + \sqrt{(E_0-I)^2 - \Delta E^2}(\cos^2\theta - \sin^2\theta) - \sqrt{2E_0}(\sqrt{E_0 - I + \Delta E} + \sqrt{E_0 - I - \Delta E})\cos\theta\right]^{1/2}$	

[a] With energies also in a.u.
[b] For determination of momentum densities in valence states of gaseous atoms and molecules.

The matrix element connecting the initial and final states is

$$\int \Phi^* \, e^{-i\boldsymbol{k}_A \cdot \boldsymbol{r}} \, e^{-i\boldsymbol{k}_B \cdot \boldsymbol{r}_B} \cdot \sum_{j=1}^{Z} \frac{-\varepsilon^2}{|\boldsymbol{r} - \boldsymbol{r}_j|} \, \Psi \, e^{i\boldsymbol{k}_0 \cdot \boldsymbol{r}} \, d\boldsymbol{r}_1 \, d\boldsymbol{r}_2 \ldots d\boldsymbol{r}_Z \, d\boldsymbol{r} . \quad (2)$$

The integration over $\boldsymbol{r}$, the coordinate of the incident electron, was done by Bethe [13] giving the result

$$\int e^{i(\boldsymbol{k}_0 - \boldsymbol{k}_A)\cdot \boldsymbol{r}} \sum_{j=1}^{Z} \frac{-\varepsilon^2}{|\boldsymbol{r} - \boldsymbol{r}_j|} \, d\boldsymbol{r} = \frac{4\pi}{|k_0 - k_A|^2} \sum_{j=1}^{Z} e^{i(\boldsymbol{k}_0 - \boldsymbol{k}_A)\cdot \boldsymbol{r}_j} . \quad (3)$$

The result on the left-hand side is the product of a term involving only the momentum transferred by the incident electron to the target and a term involving only the coordinates of the electrons in the target atom or molecule. This means that the details of the collision can be separated from the structure of the target. If we further make the assumption that only the target electron participates in the collision, the binary-encounter approximation, only the term for electron B remains in the summation over the Z electrons in the target, and we can rewrite the matrix element as

$$\frac{4\pi}{|k_0 - k_A|^2} \langle \Phi | \, e^{i(\boldsymbol{k}_0 - \boldsymbol{k}_A - \boldsymbol{k}_B)\cdot \boldsymbol{r}_B} \, | \Psi \rangle . \quad (4)$$

The next simplifying assumption is the representation of both the wave function for the target atom and the residual ion as the product of one-electron functions, the target Hartree-Fock assumption. The application of this to the above formula gives

$$\frac{4\pi}{|k_0 - k_A|^2} \langle \Phi | \Psi_l \rangle \langle e^{i\boldsymbol{q}\cdot \boldsymbol{r}_B} | \phi_l(\boldsymbol{r}_B) \rangle \cdot \delta(E_0 - E_{ion} + k_0^2 - k_A^2 - k_B^2) , \quad (5)$$

where the first integral is the overlap of the residual-ion wave function with Ψ_l, the neutral wave function minus the ejected target-electron function $\phi_l(\boldsymbol{r}_B)$. The second integral is the Fourier transform of the single-electron wave function for the ejected electron. The delta function assures that energy is conserved. The cross-section for the (e, 2e) reaction, $\sigma_{(e,2e)}$, is then proportional to the modulus-square of the above expression,

$$\sigma_{(e,2e)} = \sigma_{(e,e)} \, |\langle \Phi | \Psi_l \rangle|^2 \, \varrho_l(\boldsymbol{q}) . \quad (6)$$

Here $\sigma_{(e,e)}$ is the Rutherford cross-section, which becomes the Mott cross-section when exchange is taken into account. The modulus-square of the overlap integral is called the spectroscopic factor, a measure of the probability that the residual-ion wave function has a hole in the initial-state orbital l. Finally, the term $\varrho_l(\boldsymbol{q})$ is the momentum density.

At this point it is important to review the approximations that have led to this formula and to consider the appropriate experimental regimes. In order to enable one to use the Born approximation the motion of the unbound electrons must be very nearly free. This will be the case when the kinetic energy of the electrons is very much larger than the ionization potential of the target electron. For the valence electrons of an atom or molecule, where the ionization potentials are of the order of 10 eV, this means that the scattered and ejected electrons should have kinetic energies in excess of 500 eV. The binary-encounter approximation ignores the interaction of the incident electron with the nucleus or nuclei, and all the electrons of the target atom or molecule with the exception of the target electron. Once again, this is a high-energy approximation that becomes increasingly accurate as the kinetic energies of the incident, scattered, and ejected electrons are increased. Here we note that the interaction between the incident electron and target electron is represented without approximation, which is not always the case for some of the higher-order approximations that seek to include the second-order interactions. Because the binary-encounter approximation leads directly to the separation of the collision kinematics from the target structure, it can be tested experimentally. The results have confirmed the accuracy of the approximation at sufficiently high kinetic energies.

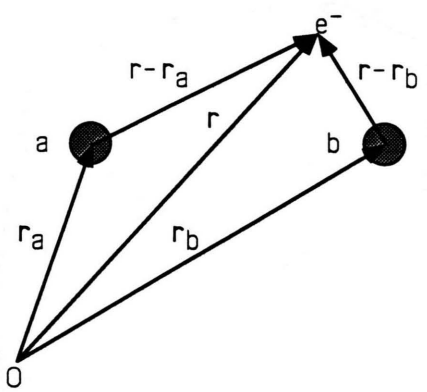

Fig. 2. Coordinate system for a simple one-electron homonuclear diatomic molecule.

Finally there is the target Hartree-Fock approximation, which is a reasonable description of the valence states. The target Hartree-Fock approximation can be improved at the expense of increased computational time through the use of configuration interaction. This partially compensates for the deficiencies in the Hartree-Fock functions, while retaining the same basic formalism.

Electron Densities in Molecules

Our interest has mostly been with the application of (e, 2e)-spectroscopy to the valence electrons of molecules, especially those molecules whose physical and chemical properties are mainly determined by a few outer valence electrons. There are interesting effects associated with the determination of the momentum densities of molecular electrons that can be illustrated by considering the momentum density for a simple one-electron homonuclear diatomic molecule with LCAO wave function Ψ. This analysis follows closely that of Coulson, and Coulson and Duncanson [14]. The two nuclei at positions a and b are located by the vectors $\boldsymbol{r}_a$ and $\boldsymbol{r}_b$ with origin at 0, Figure 2. The single electron is located by the vector $\boldsymbol{r}$, and the vectors $\boldsymbol{r}-\boldsymbol{r}_a$ and $\boldsymbol{r}-\boldsymbol{r}_b$ locate the electron with respect to the nuclear centers. The LCAO electronic wave function for the molecule, Ψ, is given by

$$\Psi_{\pm} = \frac{\psi_a \pm \psi_b}{\sqrt{2(1 \pm S_{ab})}}, \tag{7}$$

where ψ_a and ψ_b are atomic one-electron wave functions and S_{ab} is the overlap integral. The positive sign is for the symmetric (bonding) wave function and the negative sign is for the antisymmetric (antibonding) wave function. $X(\boldsymbol{q})$, the Fourier transform of Ψ, is

$$X_{\pm}(\boldsymbol{q}) = \frac{1}{(2\pi)^{3/2}} \int \Psi_{\pm}(\boldsymbol{r})\, e^{-i\boldsymbol{q}\cdot\boldsymbol{r}}\, \mathrm{d}\boldsymbol{r}\,. \tag{8}$$

This can be rewritten as

$$X_{\pm}(\boldsymbol{q}) = \frac{1}{(2\pi)^{3/2}} \int \frac{\psi_a(\boldsymbol{r}-\boldsymbol{r}_a)\, e^{-i\boldsymbol{q}\cdot(\boldsymbol{r}-\boldsymbol{r}_a)}\, e^{-i\boldsymbol{q}\cdot\boldsymbol{r}_a} \pm \psi_b(\boldsymbol{r}-\boldsymbol{r}_b)\, e^{-i\boldsymbol{q}\cdot(\boldsymbol{r}-\boldsymbol{r}_b)}\, e^{-i\boldsymbol{q}\cdot\boldsymbol{r}_b}}{\sqrt{2(1 \pm S_{ab})}}\, \mathrm{d}\boldsymbol{r}\,, \tag{9}$$

or

$$X_{\pm}(\boldsymbol{q}) = A(\boldsymbol{q})\, \frac{e^{-i\boldsymbol{q}\cdot\boldsymbol{r}_a} \pm e^{-i\boldsymbol{q}\cdot\boldsymbol{r}_b}}{\sqrt{2(1 \pm S_{ab})}}, \tag{10}$$

where

$$A(\boldsymbol{q}) = \frac{1}{(2\pi)^{3/2}} \int \psi_a(\boldsymbol{r}-\boldsymbol{r}_a)\, e^{-i\boldsymbol{q}\cdot(\boldsymbol{r}-\boldsymbol{r}_a)}\, \mathrm{d}\boldsymbol{r}\,. \tag{11}$$

The momentum density is then

$$\varrho(\boldsymbol{q}) = X_{\pm}(\boldsymbol{q})\, X_{\pm}^{*}(\boldsymbol{q}) = A(\boldsymbol{q})\, A^{*}(\boldsymbol{q}) \cdot \frac{1 \pm \cos[\boldsymbol{q}\cdot(\boldsymbol{r}_a - \boldsymbol{r}_b)]}{(1 \pm S_{ab})}\,. \tag{12}$$

The leading term is the atomic momentum density, and all of the information about the molecule is contained in the second term. In the second term the argument of the cosine is the scalar product of the electron momentum vector $\boldsymbol{q}$ and the internuclear distance vector $\boldsymbol{r}_a - \boldsymbol{r}_b$. When $\boldsymbol{q}$ is perpendicular to the internuclear axis the cosine has its maximum value and the momentum density for the bonding wave function is a maximum, while the momentum density for the antibonding wave function is zero. When $\boldsymbol{q}$ is parallel to the internuclear axis, the argument of the cosine depends on the product of the magnitudes of the product of $\boldsymbol{q}$ and the internuclear distance. For small values of $\boldsymbol{q}$ the momentum density of the bonding wave function is close to its maximum, while the antibonding wave function is near a minimum. The momentum densities as a function of $\boldsymbol{q}$ and the angle between $\boldsymbol{q}$ and the internuclear axis are shown in Fig. 3 for both the bonding and antibonding wave functions. Here we clearly see the nodal structure of the antibonding wave function reflected in the momentum density. This is not surprising, since the symmetry of the momentum-space wave function is preserved under Fourier transformation. Moreover, in the absence of an external magnetic field all momentum-space wave functions have inversion symmetry. This follows from the fact that in such a case all position-space wave functions are or can be made real. Even when the momentum densities are spherically averaged, as shown in Fig. 3, the symmetry properties of the two wave functions remain clearly distinguishable.

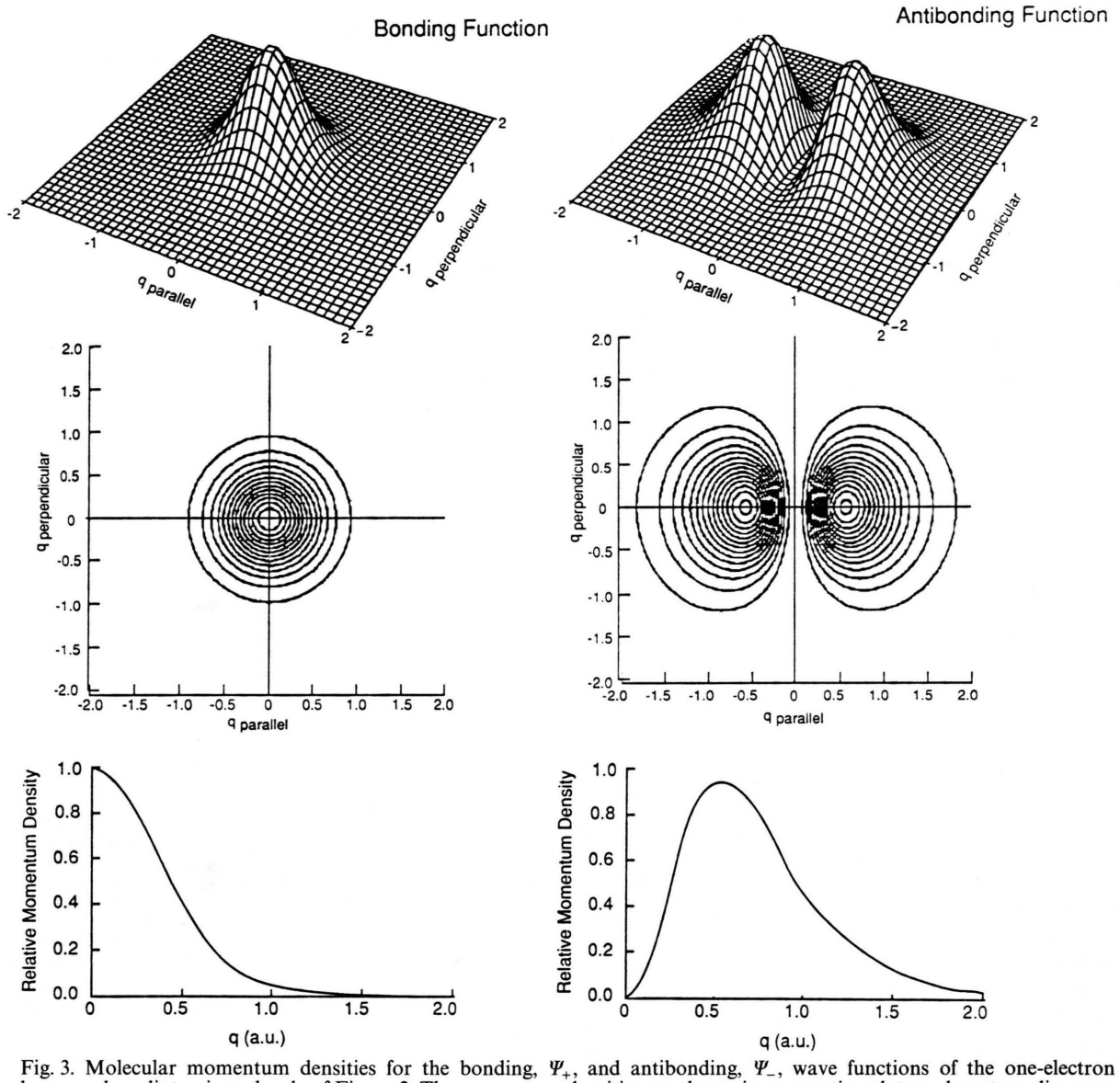

Fig. 3. Molecular momentum densities for the bonding, Ψ_+, and antibonding, Ψ_-, wave functions of the one-electron homonuclear diatomic molecule of Figure 2. The momentum densities are shown in perspective plots and contour diagrams where the independent variables are the momenta parallel and perpendicular to the internuclear axis. The spherical averages of the two densities are shown in the bottom diagrams. Hydrogen 1 s atomic wave functions have been used as basis functions, and an internuclear spacing of 1 a.u. has been assumed.

The features of this elementary example are to be found in the more complicated molecules that we shall refer to in the following examples.

Experiments

The most frequently used experimental geometry for electron momentum density measurements is the noncoplanar symmetric one. This geometry is shown schematically in Figure 4. It has two advantages; one is derived from the fact that only electrons with identical energies are accepted by the apparatus, and the other is due to the constant polar angle θ for the scattered and ejected electrons. Identical energies minimize interactions between the electrons and the residual ion, while the constant polar angle results in a

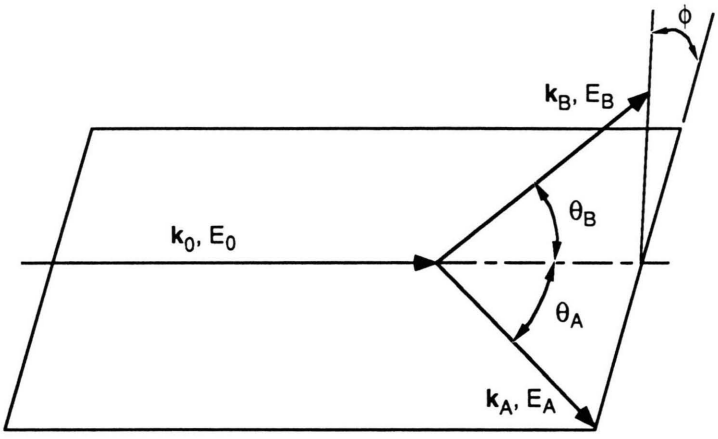

$$E_A = E_B = (E_0 - I)/2$$
$$\boldsymbol{q} = \boldsymbol{k}_0 + \boldsymbol{k}_A - \boldsymbol{k}_B$$
$$|\boldsymbol{q}| = [(2k_A \cos\theta - k_0)^2 + (2k_A \sin\theta \sin\phi/2)^2]^{1/2}$$

Fig. 4. Schematic diagram of the noncoplanar symmetric geometry.

nearly constant value for the (e, e) cross-section. This latter fact means that any variation in the (e, 2e) cross-section with change in the out-of-plane angle ϕ is almost entirely due to changes in the momentum density of the ejected electron with q. The principle disadvantage of the noncoplanar symmetric geometry is the small value of the cross-section at the values of θ usually used. In order to overcome this, asymmetric geometries where the scattering angle of the incident electron is small have been investigated with encouraging results [15, 16].

Our experimental results have been obtained with a multiple-detector noncoplanar-symmetric spectrometer shown schematically in Figure 5. In this spectrometer we take advantage of the cylindrical symmetry of the (e, 2e) collision and use fourteen separate discrete detectors to sample 49 different ϕ angles simultaneously [17]. This increases the data rate by a factor of 49 over that of a conventional two-detector spectrometer, while at the same time it eliminates the need to monitor incident current and target density. On the other hand, the fourteen detectors must be carefully calibrated, since variations in their sensitivities during the course of a measurement can result in significant errors. The energy resolution of the spectrometer is 1.4 eV and the momentum resolution 0.07 a.u. Normal operating conditions are an incident electron current of 1 to 20 microamps and a target density of 10^{12} to 10^{13} cm^{-3}.

Three Case Studies

Having established the relation between the (e, 2e) cross-section and momentum densities, we will give three examples from our work to illustrate the kinds of chemical information that can be obtained. We have concentrated on molecules whose chemical and physical properties are mostly given by a few outer valence electrons. In borazine $B_3N_3H_6$, the outermost valence electrons are π-electrons. There is some evidence that these electrons give borazine an aromatic character very much like benzene [18]. For the siloxanes, we were mainly interested in the nature of Si–O bonds and the changes in the basicity of the lone-pair electrons on the oxygen atom [19]. Finally, in our study of the weakly bound complex trimethylamine–boron trifluoride we wanted to find out how valence electrons rearrange themselves upon the formation of a chemical bond between two molecules [20].

The calculations that we use for comparison with the experimental results are done in several steps. First, the molecular geometry must be known. When bond angles and bond distances are not available from experimental data they must be calculated. We do this by locating the minimum of the total electronic energy of the molecule as a function of bond distances and angles within given symmetry constraints. These are SCF calculations with medium-size basis sets with two STOs for each valence-shell atomic orbital, but only one STO for each inner-shell atomic orbital. Because atomic orbitals are distorted in a molecule, additional basis function STOs are used where the angular momentum quantum numbers are greater than the maximum for the corresponding free atom. As is common in such quantum chemistry calculations, each STO is replaced by a contracted Gaussian function that itself is a linear combination of elementary Gaussian functions with coefficients chosen to give a good

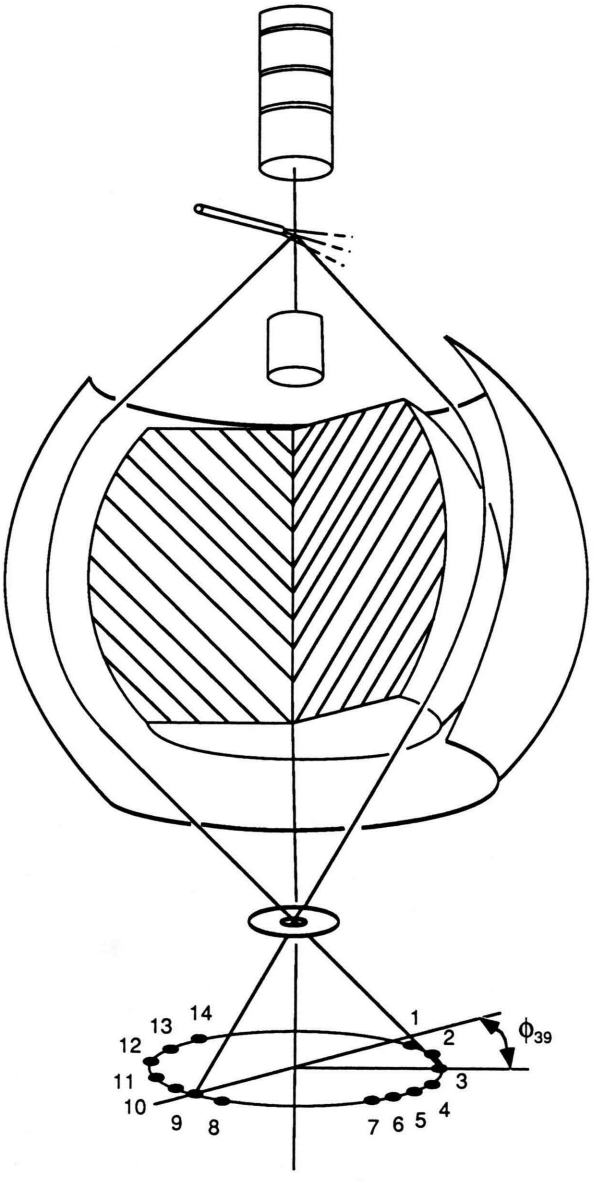

Fig. 5. Multiple-detector noncoplanar symmetric spectrometer based on a truncated spherical electrostatic analyzer. Electrons leaving the collision region at a polar angle of 45° can pass through the entrance aperture of the analyzer, but only those electrons with energies equal to the pass energy of the analyzer can reach the detectors. The pass energy is set to correspond to the ionization potential of the orbital under study. Detectors 1 through 14 are located on the focal plane of the analyzer. An (e, 2e) event with scattered and ejected electrons striking detectors 3 and 9 is shown. The out-of-plane angle, ϕ_{39}, is shown.

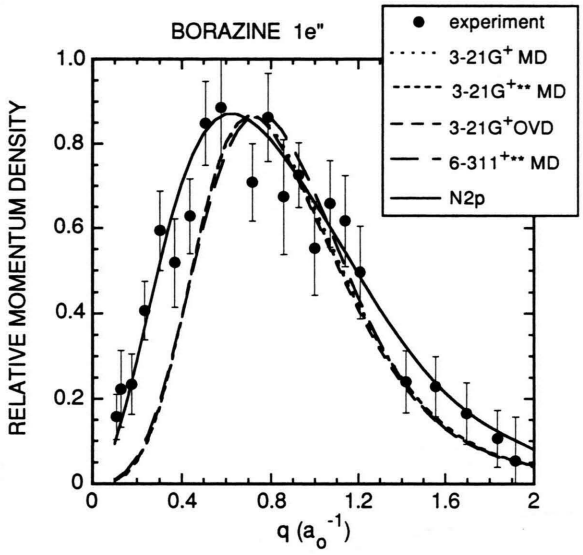

Fig. 6. Momentum densities for the highest occupied molecular orbital 1e″ of borazine, $B_3N_3H_6$. The experimental data (black circles) are compared with momentum density (MD) calculations using four different wave functions (3-21G$^+$, 3-21G$^+$**, 6-311$^+$** and atomic N2p). The fifth calculation is a full overlap density calculation (OVD) of the neutral molecule and residual ion states using 3-21G$^+$ functions.

fit to the STO. The functions we use are generally of the 3-21G* type, where each inner-shell 1s atomic orbital is represented by three elementary Gaussian functions. Two sets of functions are used for the valence-shell orbitals with one set a linear combination of two elementary Gaussian functions and the other a single Gaussian with an orbital exponent smaller than those in the set of two. The asterisk designates the addition of a single set of d-type Gaussian functions to each nonhydrogen atom to account for polarization. Additional diffuse functions are indicated by a plus-sign superscript. For the momentum density calculations we use the same basis set as for the geometry optimization calculation with the addition of diffuse Gaussian functions. The calculations can be improved by calculating the full overlap between the neutral-target state and the residual-ion state with CI wave functions. This is a considerably more difficult calculation, and at present is only justified when the simpler momentum density calculations clearly fail to reproduce the experimental data.

Borazine is often called inorganic benzene because of the analogy between its three highest occupied molecular orbitals and those of benzene. In this experiment we measured the momentum density of the

highest occupied molecular orbital of borazine, 1e″, and compared the results with a variety of calculations. The experimental results are shown in Figure 6. In the figure we show calculations using a variety of Gaussian basis sets along with the experimental data. There is a very clear difference between the calculations and theory. In this case the experimental momentum density is significantly broader than the calculations. The physical meaning of this discrepancy is best understood by going back to the relation between momentum density and charge density. The momentum density is the square of the absolute value of the momentum-space wave function, which is in turn the Fourier transform of the position-space wave function. The nature of the Fourier transformation is such that a compact function in one space transforms to a diffuse function in the other space. As a result we expect that a compact momentum density function corresponds to a diffuse charge density. Another way of looking at momentum densities is to recognize that the momentum operator is the spatial derivative in the position-space representation. Small values of momentum are associated with spatial regions where the position-space wave function is relatively flat. These are the regions in the tails of the wave functions and the regions of bonding wave functions between atoms. Large values of momentum are associated with spatial regions where the function is changing rapidly, often the region of nodes. Since anti-bonding wave functions have more nodes than bonding wave functions, we expect more high-momentum components for anti-bonding functions than bonding functions. Returning to the borazine results, we interpret the broad experimental momentum density as an indication that the charge density is not so diffuse as predicted by the calculations. In fact, if we calculate the momentum density for an isolated nitrogen 2p atomic orbital we find that the momentum density is much closer to the experimental momentum density for borazine than the full molecular orbital calculation on the molecule. Here the (e, 2e) experiment has given us valuable information about the valence electrons in borazine. In the absence of experimental results, it is not possible to investigate the details of the electronic structure directly. Energies alone are not sufficient. On the other hand, the experimental results in the absence of the calculations cannot be interpreted in a meaningful way. We need calculated momentum densities with which to compare. Parenthetically, it is interesting to note that our investigations of the influence of π-orbitals of halogen-substituted ethenes, we found that the experimental momentum densities matched the momentum densities for the isolated halogens more closely than the calculated π-electron density.

The siloxanes are the silicon analogues of organic ethers. The basicity of the siloxanes is principally due to the two pairs of lone-pair electrons on the oxygen atom. Our interest is the degree to which geometry changes the momentum densities of these electrons. Figure 7 shows experimental momentum densities for the highest occupied molecular orbital normally associated with the "lone-pair" electrons of three methylsiloxanes and the corresponding calculated momentum densities. For reference we also show the calculated momentum density for the analogous molecular orbital of water, $1b_1$. The two-peaked structure for the siloxanes is very different from the single-peak water momentum density. The multiple-peak structures in the calculated momentum densities for the highest occupied molecular orbitals for the lone-pair electrons in both the linear and cyclic siloxanes are due to the admixture of Si 3p, H 1s and C 2p atomic orbitals and the O 2pπ. The difference between the momentum densities of linear disiloxane and the 3-ring and 4-ring compounds is mostly due to the delocalization of the HOMO over the oxygens in the ring. The experimental data were difficult to obtain because of the corrosive nature of the siloxanes; nevertheless the two-peak structure predicted by the calculations is seen in the experiment. Both the HOMO and LUMO of $Si(CH_3)_3$ are predominantly C 2p in character, and this character is reflected in the HOMOs of the methylated siloxanes. This direct observation of the C 2p character of the HOMOs of the siloxanes bears directly on models for bonding in these compounds.

The final example of the application of (e, 2e)-spectroscopy to chemical problems is the donor–acceptor complex trimethylamine–boron trifluoride. This complex is formed when the lone-pair electrons on the amine interact with the empty B 2p orbital to form a bonding molecular orbital. Since trimethylamine is a stable molecule, it was possible to measure the momentum density of the N 2p electrons in the amine and then the corresponding bonding molecular orbital in the complex in order to see how the electrons rearranged themselves upon the formation of a chemical bond. Figure 8 is a correlation diagram showing how the molecular orbitals of the isolated reactant molecules interact in the formation of the molecular

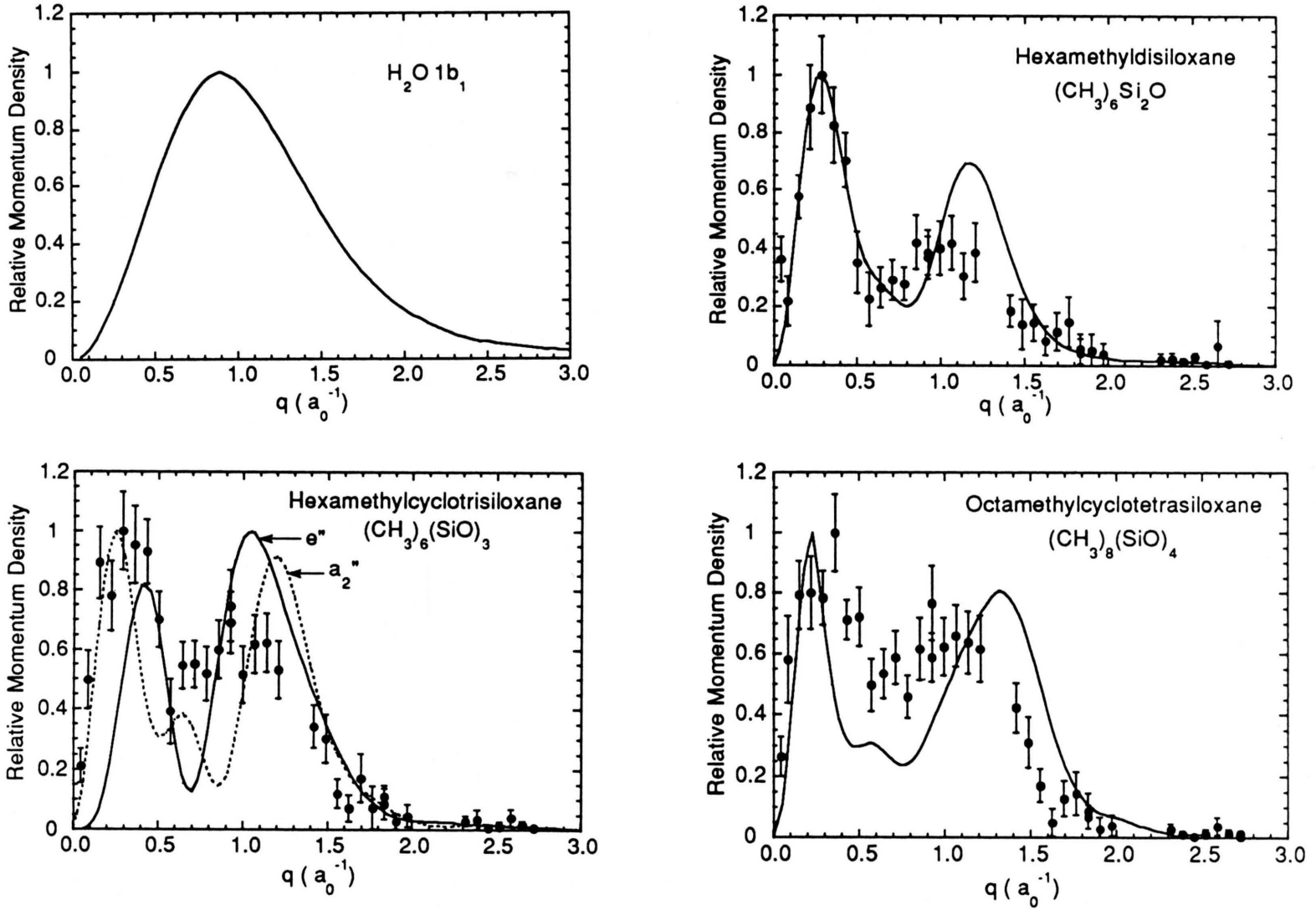

Fig. 7. Experimental and calculated momentum densities for the highest occupied molecular orbitals of hexamethyldisiloxane and octamethylcyclotetrasiloxane. Because of the energy resolution of the experiment it was not possible to separate the a_2'' highest occupied molecular orbital of hexamethylcyclotrisiloxane completely from the adjacent e″ orbital. The calculations for both orbitals are shown. The calculations are all based on 3-21G** restricted Hartree-Fock wave functions for geometries optimized at the restricted Hartree-Fock 3-21G** level. For reference the momentum density for the $1b_1$ highest occupied molecular orbital of water is also shown.

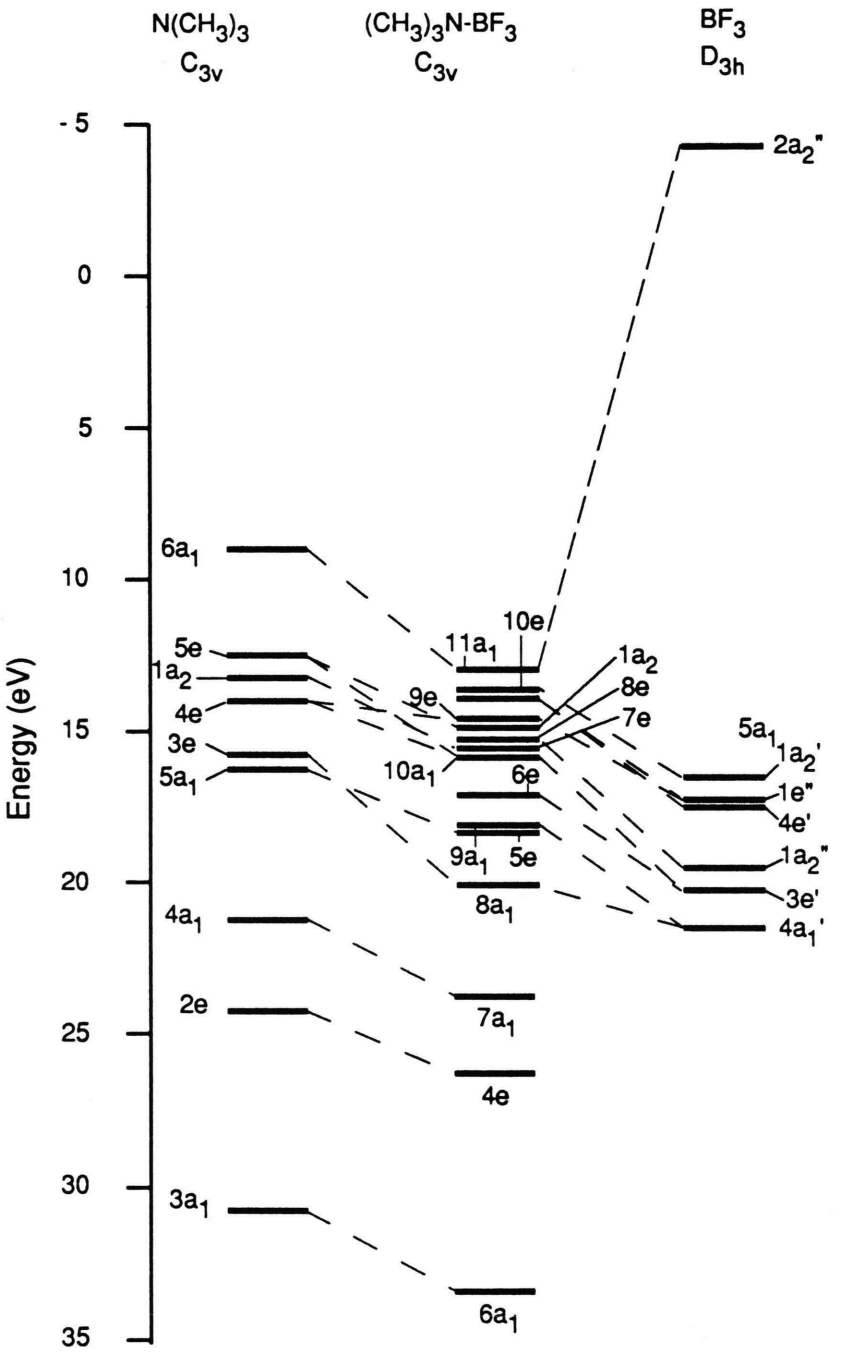

Fig. 8. Correlation diagram showing the states of trimethylamine, boron trifluoride, and the complex of the two. Bond formation occurs when charge density is donated from the $6a_1$ nonbonding highest occupied orbital of trimethylamine to the $2a_2''$ lowest unoccupied orbital of boron trifluoride.

complex. The highest occupied orbital of trimethylamine is the nonbonding $6a_1$, and the lowest unoccupied molecular orbital of boron trifluoride is the antibonding π^*, $2a_2''$. These two orbitals correlate with the $11a_1$, highest occupied orbital of the complex. The experimental and calculated momentum densities for the $11a_1$ orbital of the complex are shown in Fig. 9 along with the momentum density for the $6a_1$ orbital of the free trimethylamine. A comparison of the experimental momentum densities for the two orbitals shows the HOMO of the complex to have a significantly larger momentum density at high momentum.

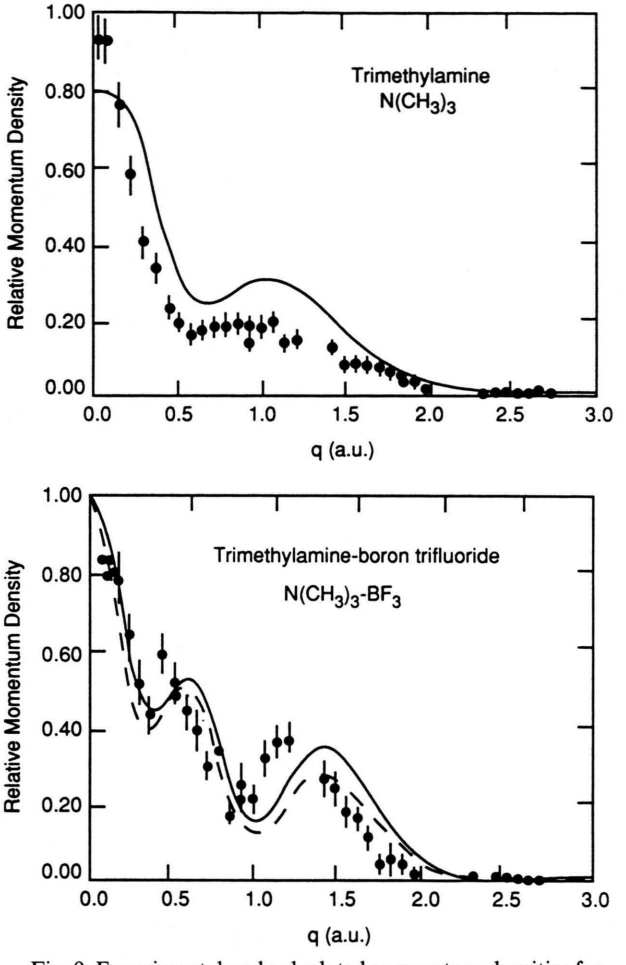

Fig. 9. Experimental and calculated momentum densities for the $6a_1$, highest occupied molecular orbital of trimethylamine and the $11a_1$ orbital of trimethylamine–boron trifluoride. For the complex, the broken line is a calculation using a 3-21G$^+$ wave function and the solid line shows the results with a 3-21G wave function.

The shape of the momentum density for the orbital of the complex has more structure than that of the free amine with peaks at momentum values of 0.44 and 1.15 a.u. We attribute the large amplitude near zero momentum to the contribution of the methyl-group hydrogen 1s orbitals. This is evidence that the electron density continues to be substantially delocalized over the methyl groups even upon the formation of a chemical bond with boron trifluoride. We attribute the increase of the high-momentum components of the momentum density of the $11a_1$ compared to the $6a_1$ to the antibonding interactions between the fluorine and nitrogen 2p orbitals. As demonstrated in the discussion of molecular momentum densities, the orbital momentum density is the product of an atomic term and an interference term. The modulation of the atomic density term by the interference term is a reflection of the symmetry of the molecule. In the case of the $11a_1$ orbital, the modulation is sufficient to produce secondary extrema in the momentum density. From this study we were able to show that the formation of the bond in the donor–acceptor complex involves more than the simple accumulation of charge density between the boron and nitrogen atoms. The experimental results, supported by the calculations, show substantial electron charge density distributed over the methyl groups along with a strong F2p–N2p antibonding interaction.

Conclusions

Because (e, 2e) spectroscopy can provide information about the momentum densities of individual atomic and molecular orbitals, it is useful for the investigation of electronic structure. The experimental progress over the last several years has resulted in increased energy and momentum resolution at the same time that statistical uncertainty has been decreased. We are currently limited by the random orientation of the targets, which averages out fine structure in the momentum densities. Nevertheless, for a large number of chemically interesting molecules, spherically averaged momentum densities, when combined with calculations, can tell us a great deal about molecular bonding.

Acknowledgement

This research has been supported by National Science Foundation grant CHE-8808589.

[1] A. E. Glassgold and G. Ialongo, Phys. Rev. **175,** 151 (1968).
[2] I. E. McCarthy and E. Weigold, Phys. Rep. C **27,** 275 (1976).
[3] Yu. F. Smirnov and V. G. Neudachin, JETP Lett. **3,** 192 (1966).
[4] R. Camilloni, A. Giardini-Guidoni, R. Tiribelli, and G. Stefani, Phys. Rev. Lett. **29,** 618 (1972).
[5] K. T. Leung and C. E. Brion, J. Electron Spectrosc. Relat. Phenom. **35,** 327 (1985). – K. T. Leung, in: Theoretical Models of Chemical Bonding (Z. B. Maksic, ed.), Springer-Verlag, Berlin 1990, Part 3.
[6] A. L. Ritter, J. R. Dennison, and R. Jones, Phys. Rev. Lett. **53,** 2054 (1984).
[7] L. J. Allen, I. E. McCarthy, V. W. Maslen, and C. J. Rossouw, Aust. J. Phys. **43,** 453 (1990).
[8] J. F. Williams and P. A. Hayes, Aust. J. Phys. **43,** 465 (1990). – P. A. Hayes, J. F. Williams, and J. Flexman, J. Electron Spectrosc. Relat. Phenom. **53,** c5 (1990).
[9] Y. Zeng, I. E. McCarthy, E. Weigold, and D. Zhang, Phys. Rev. Lett. **64,** 1358 (1990).
[10] F. W. Byron, Jr and C. J. Joachain, Phys. Rep. **179,** 211 (1989).
[11] I. E. McCarthy and E. Weigold, Electron Atom Ionization, ESM Report No. 10, The Flinders University of South Australia, internal report.
[12] H. Ehrhardt, J. Jung, G. Knoth, and P. Schlemmer, Z. Phys. D **1,** 3 (1986).
[13] H. A. Bethe, Ann. Physik **5,** 325 (1930).
[14] C. A. Coulson, Proc. Cambridge Phil. Soc. **37,** 55 (1941); C. A. Coulson, Proc. Cambridge Phil. Soc. **37,** 74 (1941); C. A. Coulson and W. E. Duncanson, Proc. Cambridge Phil. Soc. **37,** 67 (1941); C. A. Coulson and W. E. Duncanson, Proc. Cambridge Phil. Soc. **37,** 100 (1941).
[15] L. Avaldi, R. Camilloni, E. Fainelli, and G. Stefani, J. Phys. B: At. Mol. Phys. **29,** 4163 (1987).
[16] A. Lahmam-Bennani, A. Duguet, and C. Dal Cappello, J. Electron Spectrosc. Relat. Phenom. **40,** 141 (1986).
[17] R. R. Goruganthu, M. A. Coplan, J. H. Moore, and J. A. Tossell, J. Chem. Phys. **89,** 25 (1988).
[18] J. A. Tossell, J. H. Moore, K. McMillan, C. K. Subramaniam, and M. A. Coplan, J. Amer. Chem. Soc. **114,** 1114 (1992).
[19] J. A. Tossell, J. H. Moore, K. McMillan, and M. A. Coplan, J. Amer. Chem. Soc. **113,** 1031 (1991).
[20] K. McMillan, M. A. Coplan, J. H. Moore, and J. A. Tossell, J. Phys. Chem. **94,** 8648 (1990).